Discover Chemistry

RESEARCH Open Access

Screening of prospective anti-allergic compounds as a common inhibitor for different proteinaceous allergens from animal

Nutan Kumari Tudu[1†], Debabrata Das[2†], Srijita Ari[3], Subhasis Sarkar[1], Agniswar Sarkar[2] and Anindya Sundar Panja[4*]

[†]Nutan Kumari Tudu and Debabrata Das have contributed equally to this work.

*Correspondence:
Anindya Sundar Panja
biotech2ani@gmail.com
[1]Department of Biotechnology, School of Life Science, Swami Vivekananda University, Barrackpore, West Bengal, India
[2]Department of Biosciences, JIS University, 81, Nilgunj Road, Agarpara, Kolkata 700 109, India
[3]Department of Biotechnology, Burdwan Institute of Management and Computer Science, Dewandighi, Burdwan, West Bengal, India
[4]Molecular informatics Laboratory, Post Graduate Department of Biotechnology, Oriental Institute of Science and Technology, Vidyasagar University, Midnapore, West Bengal, India

Abstract

Exposure to protein-based allergens poses a growing health risk for individuals of all age groups. Already anti-allergy medications are commonly prescribed to reduce symptoms and inflammation. Allergen-specific common inhibitors against a wide spectrum of allergens may be applied to treatment. The aim of our study was to identify structurally homologous pockets present across various protein allergens and, using a similarity index, to identify for potential anti-allergic compounds that can target animal allergens. We collected and analysed a substantial dataset of a total of 62 proteinaceous allergen sequences and structures from animals. The effectiveness of 51 potential anti-allergic compounds was assessed through ADMET studies followed by high-throughput molecular docking. The AutoDock software was used to calculate the binding energies of these compounds, which helped identify the binding sites between proteinaceous allergens and potential anti-allergic agents. Further analysis of intra- and inter-sequence relationships, alongside structural examinations, showed notable structural similarities among the proteinaceous allergens of animals. Interatomic profiles of the compounds with allergens, Albiflorin and Paeoniflorigenone demonstrated the highest binding free energy ($\Delta G - 6.2 \pm 0.9$) against the catalytic pockets of proteinaceous allergens. These compounds portray theoretically as agonist molecules when interacts with TLR2 and TLR4 both. All the in silico assessments revealed finally their significant potential as both anti-allergic and anti-inflammatory agents, offering hope for more effective treatments. Moving forward, in vivo testing will be essential to confirm their efficacy and potential for widespread use.

Keywords Proteinaceous allergens, Structural homology, Anti-allergy inhibitors, ADMET, Binding free energy

1 Introduction

Allergic disorders, including asthma, rhinitis, dermatitis, and food allergies, are among the most prevalent chronic diseases globally, affecting over 30% of the world's population and exhibiting increasing trends across both developed and developing nations [1–3]. Such disorders are often triggered by proteinaceous allergens, which are antigenic

molecules capable of eliciting IgE-mediated hypersensitivity reactions upon exposure [4, 5]. Common sources of allergens include bacteria, fungi, plants, and animals, contributing to a wide spectrum of allergen diversity in both environmental and dietary contexts [6, 7]. Proteinaceous allergens commonly found when humans come into contact with domesticated mammals on farms, and in laboratories. These mammals include cats, dogs, horses, cows, rodents and, others. These allergic effects and their presence are detected by different assays, among which ELISA is the most popular [8–11]. Current therapeutic strategies largely rely on symptom management using antihistamines, corticosteroids, and leukotriene receptor antagonists [12]. Allergen-specific immunotherapy (AIT) remains the only disease-modifying treatment available; however, it is time-consuming, costly, and associated with risks of anaphylaxis and low patient compliance [13–15]. It is also important to note that Toll-like receptor (TLR) modulation influences allergic immunity. Different studies have revealed that TLR4 and TLR2 ligands agonist molecules can reduce allergic responses. These two TLRs specifically inhibit allergen-specific Th2 responses in atopic patients [16–19]. Due to structural and immunological similarities among allergens from different species commonly termed cross-reactivity, patients sensitized to one allergen may respond to structurally homologous allergens from unrelated sources [6, 20, 21]. Recent advances in computational biology and structural bioinformatics have paved the way for integrative strategies that leverage sequence analysis, structural modeling, and in silico screening for drug discovery [22–24]. Multiple sequence alignment (MSA) tools like Clustal Omega allow for the identification of conserved motifs and homologous domains across protein families [25]. When coupled with homology modeling platforms such as SWISS-MODEL, researchers can construct accurate three-dimensional protein structures, enabling structure-based drug discovery even in the absence of crystal structures [26–28]. Structural comparison through root mean square deviation (RMSD) analysis offers insight into the degree of similarity between allergen structures, which is essential for identifying conserved catalytic or binding pockets [29]. Once representative allergen models are selected, high-throughput virtual screening and molecular docking using tools like AutoDock can assess the binding affinity and orientation of ligands within active sites [30, 31]. Such approaches have been successfully applied to repurpose phytochemicals and natural products as therapeutic agents against various protein targets [32, 33]. Phytochemicals, especially flavonoids and glycosides, possess a range of biological activities including anti-allergic, anti-inflammatory, and antioxidant properties [34–36]. Compounds such as Albiflorin, Kaempferol, and Paeoniflorigenone have already demonstrated efficacy in modulating key inflammatory pathways and inhibiting histamine release, making them promising candidates for allergy intervention [37–39]. Despite the promising bioactivity of many phytocompounds, their drug-likeness and toxicity profiles must be evaluated through ADMET (Absorption, Distribution, Metabolism, Excretion, and Toxicity) analyses to ensure translational viability [40, 41]. This present study aimed to identify structurally conserved features across 62 proteinaceous allergens from animals using sequence and structural analysis. Representative allergen models were generated and validated and a library of 51 anti-allergic phytocompounds was screened using ADMET profiling and molecular docking. We also evaluated the effects of the finally screened active molecules on TLR4 and TLR2 interactions. The overall goal was to identify potential broad-spectrum inhibitors capable of interacting with conserved allergenic sites across taxonomic

domains, thereby providing a novel framework for the development of pan-allergen therapeutics. Different proteinaceous animal allergens used to build a pocket similarity index to explore the binding affinity of unique anti-inflammatory active compounds capable of inhibiting multiple animal allergens.

2 Materials and methods

The overall experimental workflow is schematically represented in the Supplementary Fig. 1. This figure displays a graphical overview of the study design, including sequence retrieval, conserve and active pockets identification, structural modeling, ligand screening, molecular docking, and finally molecular dynamics simulation.

2.1 Sequence retrieval and multiple sequence alignment

The Protein Data Bank (https://www.rcsb.org/) is a significant data resource for collecting 3D structures of proteins, including animal allergens. This retrieval was conducted after cross-referencing with indexed literature in PubMed-NCBI (https://pubmed.ncbi.nlm.nih.gov/) and the Allergome database (https://www.allergome.org/index.php). A total of 62 proteinaceous animal allergen sequences were collected from the UniProt database (https://www.uniprot.org/), all details, including sequence length, were documented. The allergens are listed in Supplementary Table 1. Multiple Sequence Alignment (MSA) was performed separately for each taxonomic group, such as *Felis catus* and *Canis familiaris*, using Clustal Omega [42] (https://www.ebi.ac.uk/Tools/msa/clustalo/) for the identification of conserved motifs and homologous regions across allergens within each group. Groupwise MSAs were performed to identify conserved residues and structurally important common pockets, which guided the exploration of potential ligand -binding sites.

2.2 Homology modeling and structural validation

The conserved sequence regions obtained using MSA Clustal Omega (https://www.ebi.ac.uk/) and the selected conserved peptide sequences were used to generate three-dimensional structural models through homology modeling using the SWISS-MODEL server (https://swissmodel.expasy.org/) [26, 27, 43–45]. Each model was assessed for stereochemical quality using Ramachandran plots generated by PROCHECK [46, 47]. By utilizing the Computed Atlas of Surface Topography of Proteins (CASTp; version 3.0.) the active zones or pockets were identified from previously modelled structures [48]. Only models with > 90% residues in the most favored regions were selected for further analysis (Supplementary Table 16). Human TLR2 (2Z7X) and TLR4 (4G8A) structures of the target proteins were obtained from the RCSB protein database (https://www.rcsb.org).

2.3 Structural comparison and RMSD analysis

To assess structural similarity within each group, Root Mean Square Deviation (RMSD) values were calculated between the modeled structures. RMSD calculations were carried out using PyMOL version 3.1.6.1 [49]. The structure with the lowest average RMSD when compared to others in its group was selected as the representative model for further molecular docking.

2.4 Ligand selection and ADMET screening

A literature review yielded 51 potential anti-allergic compounds. These compounds were retrieved from the PubChem database (https://pubchem.ncbi.nlm.nih.gov/) and subjected to ADMET (Absorption, Distribution, Metabolism, Excretion, and Toxicity) profiling usingADMETlab 2.0 (https://admetmesh.scbdd.com/) [40, 50]. Compounds showing optimal pharmacokinetic properties and minimal predicted toxicity were shortlisted for docking studies. We evaluated Physicochemical parameters, where acceptable compounds had a molecular weight of < 500 Da, LogP < 5, hydrogen bond donors < 5, and hydrogen bond acceptors ≤ 10. Further properties like volume, TPSA, nROT, molar refractivity, and LogS were also evaluated. Absorption criteria included values for Pgp inhibitor status, Pgp substrate status, and HIA values in the range 0–0.3. Also, the Caco-2 permeability values ≥ − 5.15 were considered favorable while log Kp and PAMPA permeability were also evaluated. Distribution parameters included acceptable blood—brain barrier permeation values in the range 0–0.3, while VDss and fraction unbound were evaluated without strict limits. Metabolic profiling included acceptable probabilities between 0–1 for CYP1A2 inhibitor and substrate activity; other CYP isoforms were also screened. Excretion parameters showed acceptable ranges for clearance ≥ + 5 and half-life values in the range 0–0.3. Toxicity parameters accepted values in the range 0–0.3 for hERG blockers, H-HT, AMES toxicity, FDAMDD, Oral Acute toxicity, carcinogenicity, and bioavailability score. Hematotoxicity, along with genotoxicity, immunotoxicity, neurotoxicity, ototoxicity, nephrotoxicity, cytotoxicity assays, and stress response pathways, were also evaluated.

2.5 Molecular docking

Selected allergen structures and filtered ligands were prepared for docking using AutoDock 4.2.6 Tools. Protein structures were optimized by removing water molecules, adding polar hydrogen, and assigning Kollman charges. Ligands were converted using Open Babel [51]. Docking simulations were performed using AutoDock4 [30]. Human TLR2 (2Z7X) and TLR4 (4G8A) high-resolution structures were downloaded and docked with the finally screened molecules [52, 53]. The binding affinity (ΔG) and docking scores were recorded, and binding interactions were visualized using Biovia Discovery Studio (DS2021 (Version 25.1.0.24284) [Discovery Studio (DS) 2021; Accelrys, San Diego, CA, USA].

2.6 Molecular dynamics simulation

Molecular dynamics (MD) simulations were conducted for four complexes: Paeoniflorigenone with allergen proteins (A6 and A10), and Albiflorin with TLR2 and TLR4, using the GROMACS package. The complexes were solvated in TIP3P water with periodic boundary conditions and a 10 Å buffer. Each protein–ligand complex was centered within a cubic simulation box ($90.0 \times 90.0 \times 90.0$ nm^3) and parameterized using the CHARMM27 force field. The system was subsequently solvated with the SPC water model. To achieve electrostatic neutrality, appropriate numbers of Na^+ and Cl^- ions were introduced by replacing solvent molecules, thereby counterbalancing the net charge of the system [49, 54–56]. Energy minimization was followed by 100 ns NPT simulations at 300 K and 1 atm, using Nosé -Hoover temperature coupling method and Martyna-Tobias-Klein barostat with PME electrostatics (0.8 Å grid spacing). MD Trajectory

and energy data were saved every 1000 ps using the gmx rms module [57]. Structural integrity was monitored by RMSD, RMSF, radius of gyration (Rg), and hydrogen bond analysis [58]. Binding energies for all the four complexes were also calculated using the GMX_MMPBSA module from the final 100 ns of the simulation trajectories [56, 59, 60] The binding free energy (ΔG_binding) is calculated as follows: ΔG_binding = ΔE_MM + ΔG_ps + ΔG_nps – TΔS. Here, ΔE_MM (ΔE_MM = ΔE_vdW + ΔE_EE) represents the molecular mechanics energy in vacuum, comprising van der Waals (ΔE_vdW) and electrostatic (ΔE_EE) interaction energies. ΔG_ps denotes the polar solvation free energy, ΔG_nps represents the nonpolar solvation free energy, and TΔS corresponds to the entropic contribution to binding.

3 Result

3.1 Identification of conserve pockets

A total of 62 animal allergenic protein sequences were retrieved from the UniProt database (Supplementary Table 1). Multiple sequence alignment (MSA) conducted independently for each group using Clustal Omega revealed conserved motifs and homologous regions across members within each group (Supplementary Fig. 2–14). These conserved sequence regions were selected for homology modeling using the SWISS-MODEL server. Only models with more than 90% of residues in the most favored regions of the Ramachandran plots were retained. To evaluate structural similarity among homologous allergens, Root Mean Square Deviation (RMSD) values were calculated using PyMOL. Structural alignments revealed varying degrees of intra-group homology. The structure demonstrating the lowest average pairwise RMSD was selected as the representative model, reflecting the most conserved fold within that group (Supplementary Table 3–15). Following RMSD-based filtration, 13 representative structures were retained for further docking analysis (Fig. 1). For animal allergens we selected 13 representative structures from UniProt entries P30922, P49822, P35747, P02769, Q7YS85, P49064, with some entries occurring multiple times due to their presence in distinct allergenic isoforms or properties (Supplementary Table 2). The length of the allergenic peptide sequences was 44 ± 7 amino acids. The six proteinaceous animal allergens from *Canis familiaris, Equus caballus, Bubalus bubalis, Felis catus* and two *Bos taurus* represented the 13 allergens active pockets.

These representative structures formed the core dataset for subsequent molecular docking analyses with minimizing redundancy.

3.2 ADMET result

Subsequently, 51 phytochemical compounds with reported anti-allergic or anti-inflammatory properties were compiled from the literature and retrieved from the PubChem database. These compounds were subjected to in silico ADMET screening using the ADMETlab 2.0 platform to assess drug-likeness, pharmacokinetic profiles, and toxicity risks (Supplementary Table 17). Based on the screening outcomes, six phytochemicals—Epicatechin, Kaempferol, Tectorigenin, Albiflorin, Paeoniflorigenone, and Hydrobromide —exhibited favorable ADMET properties and were shortlisted for further molecular docking studies against the selected allergen models. After ADMET evaluation both Paeoniflorigenone and albiflorin demonstrated favorabale pharmacokinetic and safety profiles. Paeoniflorigenone met criteria such as balanced physicochemical

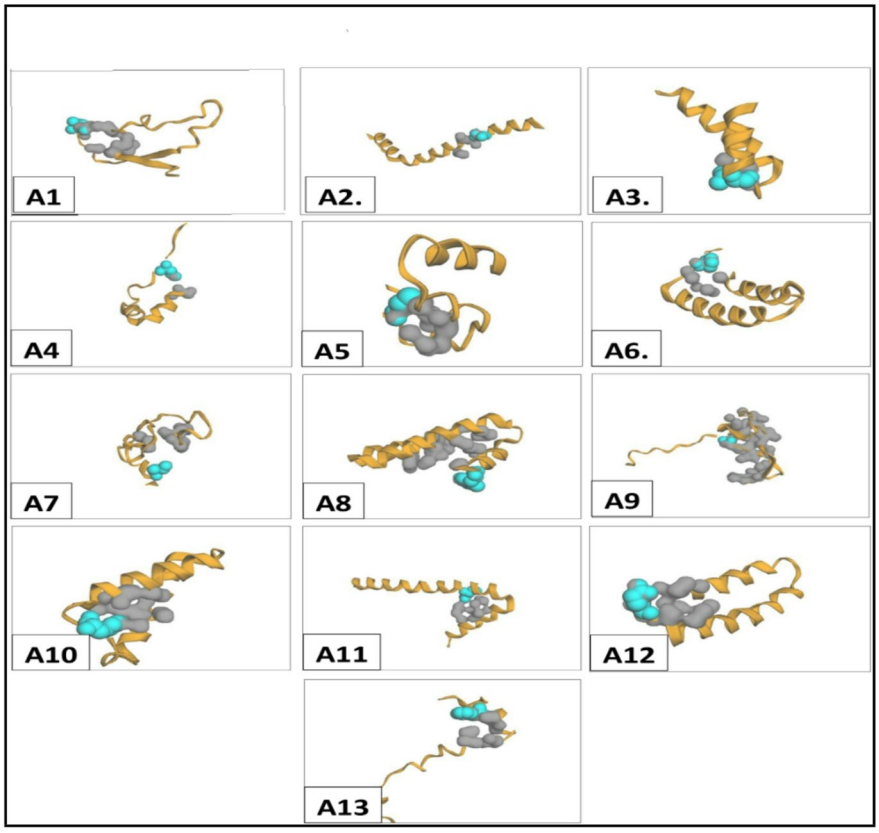

Fig. 1 13 conserved structures selected based on the sequence and structural similarity, A1–A13 represents the conserve sequence found during the MSA. CPK fill displays the active pockets

characteristics using different drug likeliness rules including Golden triangle filter. Others parameters, such as appropriate molecular weight, moderate lipophilicity, good permeability, acceptable clearance values, and low predicted toxicity probabilities, were also satisfied. Albiflorin also met the same parameters except for the GSK filter. Evidently, these compounds indicated desirable absorption-related characteristics; manageable CYP 1A2 interactions; and desirable distribution characteristics. Critically, the results of these predictions on hERG, AMES mutagenicity, skin sensitization, carcinogenic effects, respiratory toxicity, and rat acute oral toxicity were within the acceptable range. Low probabilities of hematotoxicity, genotoxicity, immunotoxicity, and nephrotoxicity were observed. These observations suggest that among the 51 compounds, Paeoniflorigenone and albiflorin both met acceptable drug-like characteristics and safety profiles, making them potential lead compounds for subsequent molecular docking studies.

3.3 Docking analysis

In this docking study, a total of 78 interactions were observed between 13 allergenic protein and 6 selected phytochemicals. The docking scores of selected phytochemicals with allergens and related proteins from different Animal sources revealed diverse binding affinities. The same protein, such as Chitinase-3-like protein, from different sources also exhibited structural deviations (Supplementary Tables 3–15). Binding Energy of 13 conserved pocket of different animal allergens with Albiflorin, Tectorigenin, Epicatechin,

Paeoniflorigenone, Kaempferol, and Hydrobromide are represented in Fig. 2, where ΔG is kcal/mol.

In *Bos taurus* (Bovine), the Chitinase-3-like protein 1 (UniProt ID: P30922) (A1) showed moderate interactions with the selected phytochemicals. In the first docking, Albiflorin exhibited the highest ΔG (– 6.4 ± 0.1), followed by Tectorigenin (– 6.0 ± 0.1), Epicatechin and Paeoniflorigenone (both – 5.9 ± 0.1), Kaempferol (– 5.8 ± 0.1), and Hydrobromide (– 5.4 ± 0.1). In a second entry for the same protein (A4), Paeoniflorigenone showed a highest ΔG score (– 6.1 ± 0.1), followed by Albiflorin (– 5.9 ± 0.1), Epicatechin (– 5.8 ± 0.1), Kaempferol (– 5.6 ± 0.1), Tectorigenin (– 5.4 ± 0.1), and Hydrobromide (– 5.5 ± 0.1). The bovine serum albumin (UniProt ID: P02769) (A6) showed highest ΔG interactions, with Paeoniflorigenone scoring the highest (– 7.1 ± 0.2) in the first docking, followed by Kaempferol and Albiflorin (both – 6.41 ± 0.1), Tectorigenin (– 6.2 ± 0.1), Epicatechin (– 6.1 ± 0.1), and Hydrobromide (– 6.1 ± 0.1). In a second instance (A13), the highest ΔG was observed with Kaempferol (– 7.0 ± 0.2), followed by Epicatechin (– 6.8 ± 0.1), Tectorigenin (– 6.6 ± 0.1), Paeoniflorigenone (– 6.3 ± 0.1), Albiflorin (– 6.0 ± 0.1), and Hydrobromide (– 6.0 ± 0.1). In *Canis lupus familiaris* (Dog), the allergen Albumin (UniProt ID: P49822) was docked multiple times. In the first run (A2), Paeoniflorigenone showed the highest ΔG (– 6.2 ± 0.1), followed by Epicatechin (– 5.9 ± 0.1), Albiflorin (– 5.6 ± 0.1), Kaempferol (– 5.5 ± 0.1), Tectorigenin (– 5.0 ± 0.1), and Hydrobromide (– 5.4 ± 0.1), represented in Fig. 2. In another instance (A5), Epicatechin and Kaempferol scored higher (– 6.4 ± 0.01 and – 6.3 ± 0.1 respectively), followed by Albiflorin (– 6.0 ± 0.1), Paeoniflorigenone (– 5.8 ± 0.1), Tectorigenin (– 5.7 ± 0.1), and Hydrobromide (– 5.2 ± 0.1). In a third docking entry (A 10), the highest ΔG was observed with Paeoniflorigenone (– 7.0 ± 0.2) and Albiflorin (– 6.6 ± 0.2), followed by Kaempferol (– 6.1 ± 0.1), Tectorigenin and Epicatechin (both at – 5.8 ± 0.1), and Hydrobromide (– 6.3 ± 0.1). A final entry (A12) showed generally lower scores, with Paeoniflorigenone (– 5.3 ± 0.1), Albiflorin (-5.5 ± 0.1), Kaempferol (– 5.2 ± 0.1), Tectorigenin (– 5.1 ± 0.1), Epicatechin (– 5.0 ± 0.1), and Hydrobromide (– 4.7 ± 0.1). In *Equus caballus*

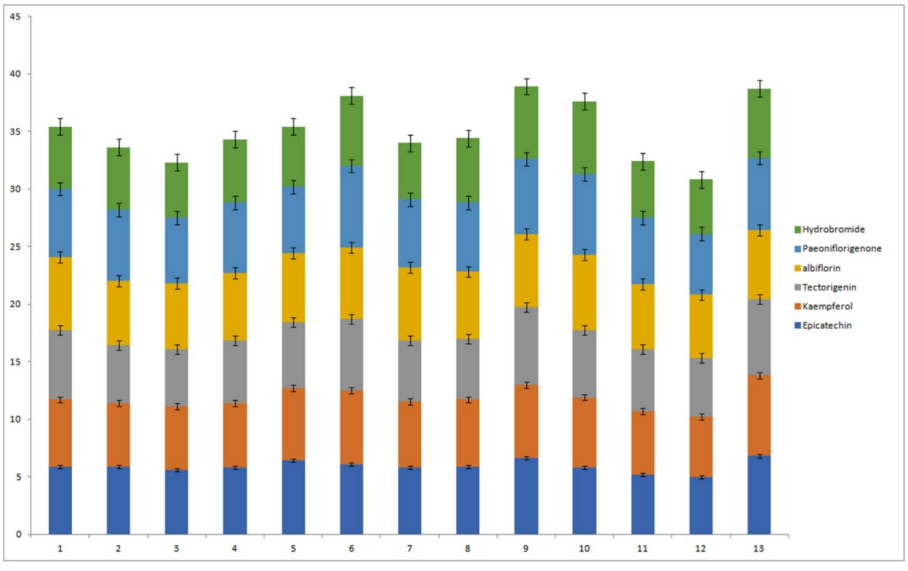

Fig. 2 Graphical representation of Binding Energy (X axis) of 13 conserved pockets (y axis) of different animal allergens with Albiflorin, Tectorigenin, Epicatechin, Paeoniflorigenone, Kaempferol, and Hydrobromide after docking study

(Horse), Albumin (UniProt ID: P35747) (A3) showed highest ΔG with Albiflorin and Paeoniflorigenone (both – 5.7 ± 0.1), followed by Epicatechin (– 5.6 ± 0.1), Kaempferol (– 5.5 ± 0.1), Tectorigenin (– 5.0 ± 0.1), and low ΔG score for Hydrobromide (– 4.8 ± 0.1) were noted and represented in Fig. 2. In *Felis catus* (Cat), Albumin (UniProt ID: P49064) (A8) was also docked in two instances. In the first, Paeoniflorigenone scored – 6.0 ± 0.1, Kaempferol and Epicatechin both had – 5.8 ± 0.1, followed by Albiflorin (– 5.8 ± 0.1), Tectorigenin (– 5.3 ± 0.1), and Hydrobromide (– 5.6 ± 0.1). In the second docking (A11), the lowest overall scores were recorded: Paeoniflorigenone (– 5.8 ± 0.1), Albiflorin (– 5.6 ± 0.1), Tectorigenin (– 5.4 ± 0.1), Kaempferol (– 5.5 ± 0.1), Epicatechin (– 5.2 ± 0.1), and Hydrobromide (– 4.9 ± 0.1). In *Bubalus bubalis* (Domestic water buffalo), Chitinase-3-like protein 1 (UniProt ID: Q7YS85) (A7) showed varied interactions.

In the first entry, Albiflorin showed the highest ΔG (– 6.4 ± 0.1), followed by Kaempferol (– 5.7 ± 0.1), Epicatechin and Paeoniflorigenone (both – 5.9 ± 0.1), Tectorigenin (– 5.3 ± 0.1), and Hydrobromide (– 4.9 ± 0.1). In a second docking of the same protein (A9), higher scores were seen with Epicatechin (– 6.6 ± 0.1), Tectorigenin (– 6.7 ± 0.1), Kaempferol (– 6.4 ± 0.1), Albiflorin (– 6.4 ± 0.1), Paeoniflorigenone (– 6.5 ± 0.2), and Hydrobromide (– 6.3 ± 0.1). After observing the ΔG score (higher the score more stable the complex) throughout all the interactions we screened Albiflorin and Paeoniflorigenone (Supplementary Table 19) for further docking interaction and molecular dynamics analysis.

3.4 Docking interaction and MD analysis

To assess the dynamic stability of Albiflorin and Paeoniflorigenone with animal allergen proteins, a total of 26 molecular dynamics (MD) simulations were performed using GROMACS 2021. Each simulation was carried out for duration of 100 ns under explicit solvent conditions. 26 protein–ligand complexes were selected based on their docking scores. Structural stability was evaluated using root mean square deviation (RMSD) and root mean square fluctuation (RMSF) analyses. The objective was to verify whether Albiflorin and Paeoniflorigenone maintained a stable binding conformation throughout the 100 ns simulation and to identify any regions of flexibility or conformational drift.

For the A1—Albiflorin complex, interacted primarily through conventional hydrogen bonding with GLN 2, SER 3, PHE 34, LEU 35, along with Alkyl interaction with CYS 4, ALA 5. For the A2-Albiflorin complex, interacted through conventional hydrogen bond with ARG 24, π-Alkyl bond with LYS 28, ILE 31, ARG 34. For the A3-Albiflorin complex, also interacted through convention hydrogen bond with LEU 11, GLN 12, CYS 14, and π–π Stacked interaction as well as π-Alkyl interaction with PHE 16For A4-Albiflorin complex we observed conventional hydrogen bond with ALA 22, unfavorable acceptor-acceptor interaction with VAL 8, Alkyl as well as π Alkyl interaction with PHE 18, PHE 31, ILE 32. (Supplementary Fig. 15).

For A5–Albiflorin complex conventional hydrogen bond with LYS 1, ARG 26, Unfavorable Donor-Donor interaction with CYS 3 and π-Alkyl with CYS 34 was observed. For A6–Albiflorin complex conventional hydrogen bond with TYR 17, Unfavorable Donor-Donor interaction with ARG 42 and π-Alkyl interaction with MET 41 was observed. For A7–Albiflorin complex Conventional Hydrogen Bond interaction with LEU 34, ARG 36, SER 42, Carbon Hydrogen Bond interaction with HIS 30 and π-Alkyl bond interaction with VAL 28, ALA 41 was observed. For A8–Albiflorin complex Conventional Hydrogen

Bond interaction with SER 4, ARG 46, Carbon Hydrogen Bond interaction with ALA 50 and π-Alkyl bond interaction with LEU 23, LEU 27 was observed. (Supplementary Fig. 16).

For A9—Albiflorin complex Conventional Hydrogen Bond interaction with ASP 53, Carbon Hydrogen Bond interaction with GLU 50, Unfavourable Donor-Donor bond with GLN 38 and π-Alkyl bond interaction with ILE 35, PHE 54 was observed. For A10–Albiflorin complex Conventional Hydrogen Bond interaction with ARG 19, Carbon Hydrogen Bond interaction with PHE 8, π-Alkyl bond interaction with ILE 39 was observed. For A11–Albiflorin complex Conventional Hydrogen Bond interaction with ASN 26, ARG 45, LYS 49, π-Alkyl bond interaction with PRO 19, LEU 22, LEU 42 was observed. For A12–Albiflorin complex Conventional Hydrogen Bond interaction with ASP 35, unfavourable Donor-Donor bond with LYS 16, π-Alkyl bond interaction with VAL 39 and π -Cation LYS 13 was observed. For A13–Albiflorin complex π-σ interaction with LEU 9, TYR 15, π-Alkyl bond interaction with VAL 16 was observed. (Supplementary Fig. 17).

In the A1—paeoniflorigenone complex, a conventional hydrogen bond interaction with ILE31 and an alkyl interaction with PRO33 were identified. Similarly, in the A2–paeoniflorigenone complex, a hydrogen bond with PHE10 and π-alkyl interactions with ILE7 and PHE13 were observed. The A3—paeoniflorigenone complex exhibited hydrogen bonds with SER8 and CYS14, along with an Amide–π stacking interaction involving SER8. In the case of the A4–paeoniflorigenone complex, π – π stacking with PHE18 and alkyl interactions with ALA22 and ARG28 were observed. (Supplementary Fig. 18).

In the A5—paeoniflorigenone complex (Supplementary Fig. 19), a conventional hydrogen bond interaction with LYS 1 and an Unfavorable Donor-Donor with PRO33 were identified. Similarly, in the A6–paeoniflorigenone complex, a conventional hydrogen bond with TYR 17 and π-alkyl interactions with VAL 20, LEU 34, MET 41, VAL 45 was observed. The A7–paeoniflorigenone complex shows conventional hydrogen bonds with LEU 34, along with a π–σ interaction involving PHE 35 and one Alkyl interaction with ALA 41. In the case of the A8–paeoniflorigenone complex, π-Alkyl interactions with PHE 12, LEU 23 and LEU 27 were observed.

After simulation A9—paeoniflorigenone complex, a conventional hydrogen bond interaction with TYR 17, GLY 27, ALA 28, a π–π stacked interaction with TYR 17 and a π-Alkyl interaction with ILE 30 were identified. Similarly, in the A10–paeoniflorigenone complex, conventional hydrogen bond with PHE 8, PHE 12 and π-alkyl interaction with PHE 8 and π -Cation bond with ARG 19 were observed. The A11–paeoniflorigenone complex shows conventional hydrogen bonds with ASN 26, along with a π–π stacked interaction involving PHE 30, PHE 38 and one Alkyl interaction with VAL 23. In the case of the A12–paeoniflorigenone complex, conventional hydrogen bonds with CYS 22, ARG 29, π-Alkyl interactions with LEU 14 and ALA 33 were observed. In the A13–paeoniflorigenone complex, a π–σ interaction with LEU 9 and a π-Alkyl interaction with VAL 16 was observed. (Supplementary Fig. 20).

Albiflorin and Paeoniflorigenone consistently resulted significant docking score, among them chain A6 (sp|P02769|ALBU_BOVIN: Bos taurus) and A10 (sp|P49822|ALBU_CANLF Canis familiaris) resulted high binding score – 7.1 kcal\mol and – 7.0 kcal\mol in case of Paeoniflorigenone (Fig. 3). According to the result we analysed stability index through 100 ns simulation.

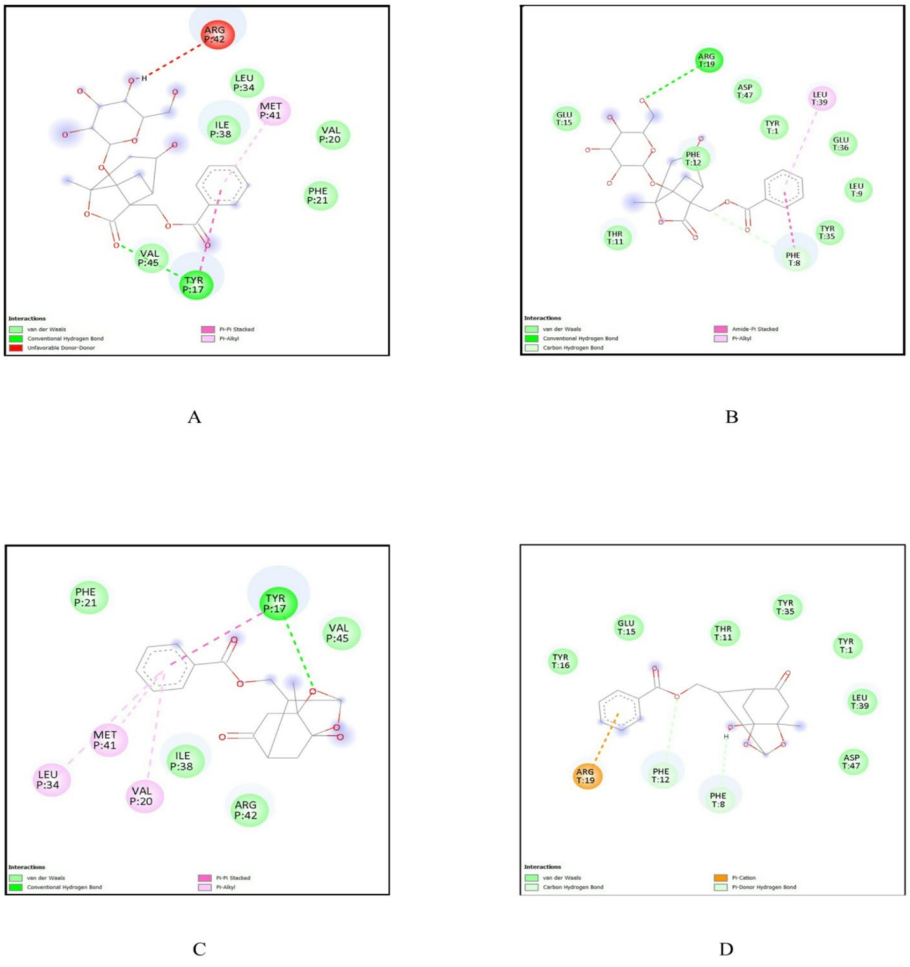

Fig. 3 Binding profile of the two bioactive compounds from *Paeonia lactiflora* with the allergen protein of A6 (Allergen from *Bos taurus*) and A10 (Allergen from *Canis familiaris*). (**A**) A6 Albiflorin binding complex (**B**) A10 Albiflorin binding complex (**C**) A6 Paeoniflorigenone binding complex (**D**) A10 Paeoniflorigenone binding complex

3.5 Docking analysis Albiflorin and Paeoniflorigenone with TLR2& TLR4

Interacting residues and interface surface areas were analyzed from the best docking complexes. The interacting residues were filtered based on hydrogen bonds and charged residues present into the complex, which specifically influence binding stability and specificity. In this study, molecular docking was performed and the binding pockets exhibiting the best binding affinities were selected out of 6 active pockets. Selected Albiflorin and Paeoniflorigenone were further analysed as the top compounds, BIOVIA Discovery Studio was used to visualize and represent the binding sites, as shown in Fig. 4.

Docking results of Albiflorin and Paeoniflorigenone with TLR2 and TLR4 showed interactions, Albiflorin showed strong affinity for TLR2 ($\Delta G = -8.0$ kcal/mol) through hydrogen bonds and hydrophobic interactions with residues such as ASN, TYR, and ASP. In case of TLR4, an even stronger binding affinity ($\Delta G = -9.0$ kcal/mol) was observed, stabilized by interactions with ASP, ASN, and TYR residues. But, case of Paeoniflorigenone displayed weaker affinities, – 5.7 kcal/mol for TLR2 and – 6.5 kcal/mol for TLR4, showed few interactions GLU, SER, and ASN residues. Overall, Albiflorin consistently exhibited superior stabilization, particularly with TLR4, suggesting that act as a more potent modulator of TLR-mediated signalling pathways, with therapeutic potential

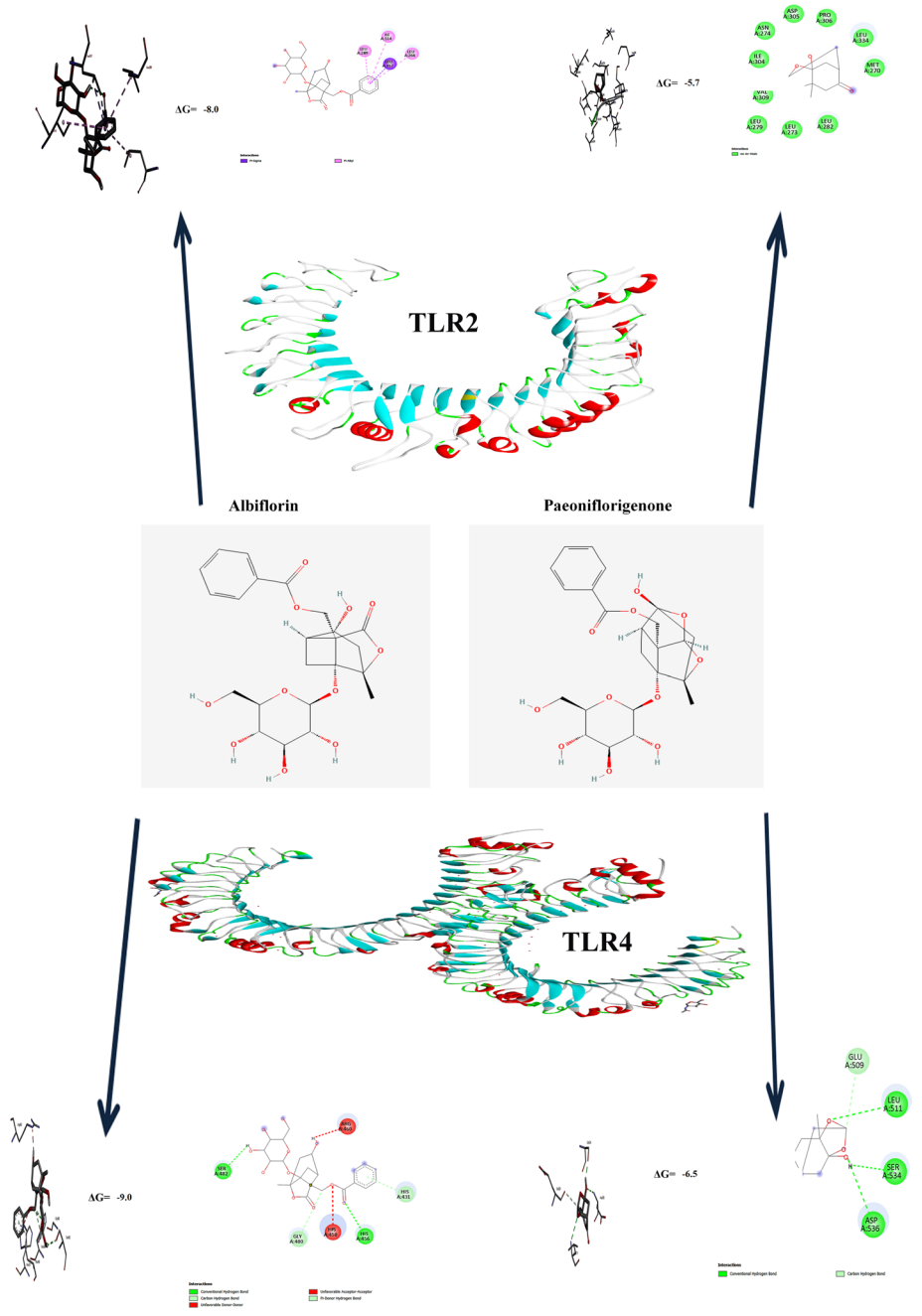

Fig. 4 Docking analysis and representation two- and three-dimensional docking interactions of Albiflorin and Paeoniflorigenone with TLR2 and TLR4

in regulating inflammation and allergic response. After docking study TLR2 and TLR 4 with Albiflorin and Paeoniflorigenone revealed that affinity and docking score is higher in case of Albiflorin, further stability analysis was conducted using 100 ns molecular dynamics (MD) simulations.

3.6 Molecular dynamics simulations of Paeoniflorigenone with A6, A10 and Albiflorin with TLR2& TLR4

MD simulations indicate the dynamic behaviour and stability of the protein ligand complexes. RMSD value for A6 (Allergen from *Bos taurus*) with Paeoniflorigenone exhibited stability throughout the simulation. The fluctuating RMSD observed at 80–90ns at 1.0–1.25 nm. In case of RMSF plots no major fluctuation were observed throughout the simulation. SASA usually used to determine the interaction between the complex and the solvent. A6 with Paeoniflorigenone complex exhibited SASA value decreased after 20ns of simulation. RG value represented lesser fluctuation after 10 ns throughout the simulation, suggesting compact protein-ligand complex. Hydrogen bond plot analysed after simulations indicating potential hydrogen bond interaction. Using GROMACS Principal Component Analysis (PCA) was analysed to visualize collective motions of a system during simulations through MD trajectories. 2D trajectory displayed dense clusters reflects structural stability of the complex (Fig. 5). RMSD value for A10 (Allergen from *Canis familiaris*) with Paeoniflorigenone exhibited stability throughout the simulation. The fluctuating RMSD observed at 60 ns at 1.0–1.52 nm.

In case of RMSF plots no major fluctuation were observed throughout the simulation. SASA usually used to determine the interaction between the complex and the solvent. A6 with Paeoniflorigenone complex exhibited stable SASA value throughout the simulation. RG value represented lesser fluctuation throughout the simulation, suggesting compact protein-ligand complex. Hydrogen bond plot after simulation indicating potential hydrogen bond interaction. Using GROMACS Principal Component Analysis (PCA) was analysed to visualize collective motions of a system during simulations through MD trajectories. 2D trajectory displayed dense clusters reflects structural stability of the complex (Fig. 6). RMSD value for TLR2 with Albiflorin exhibited stability throughout the simulation. The fluctuating RMSD observed at approx. 5 ns at 0.10–0.45 nm. In case of RMSF plots no major fluctuation were observed throughout the simulation. SASA usually used to determine the interaction between the complex and the solvent. 2TLR with Paeoniflorigenone complex exhibited stable SASA value throughout the 100 ns simulation.

RG value represented lesser fluctuation throughout the simulation, suggesting compact protein-ligand complex. Hydrogen bond plot after simulation indicating potential hydrogen bond interaction. Using GROMACS Principal Component Analysis (PCA) was analysed to visualize collective motions of a system during simulations through MD trajectories. 2D trajectory displayed dense clusters reflects structural stability of the complex (Fig. 7). RMSD value for TLR4 with Albiflorin exhibited stability throughout the simulation. The fluctuating RMSD observed at approx. 18 ns at 1.0–5.0 nm. In case of RMSF plots no major fluctuation were observed throughout the simulation. SASA usually used to determine the interaction between the complex and the solvent. 4TLR with Paeoniflorigenone complex exhibited stable SASA value throughout the 100 ns simulation. RG value represented lesser fluctuation throughout the simulation, suggesting compact protein-ligand complex. Hydrogen bond plot after simulation indicated potential hydrogen bond interactions. Using GROMACS Principal Component Analysis (PCA) was analysed to visualize collective motions of a system during simulations through MD trajectories. 2D trajectory displayed dense clusters reflects structural stability of the complex (Fig. 8).

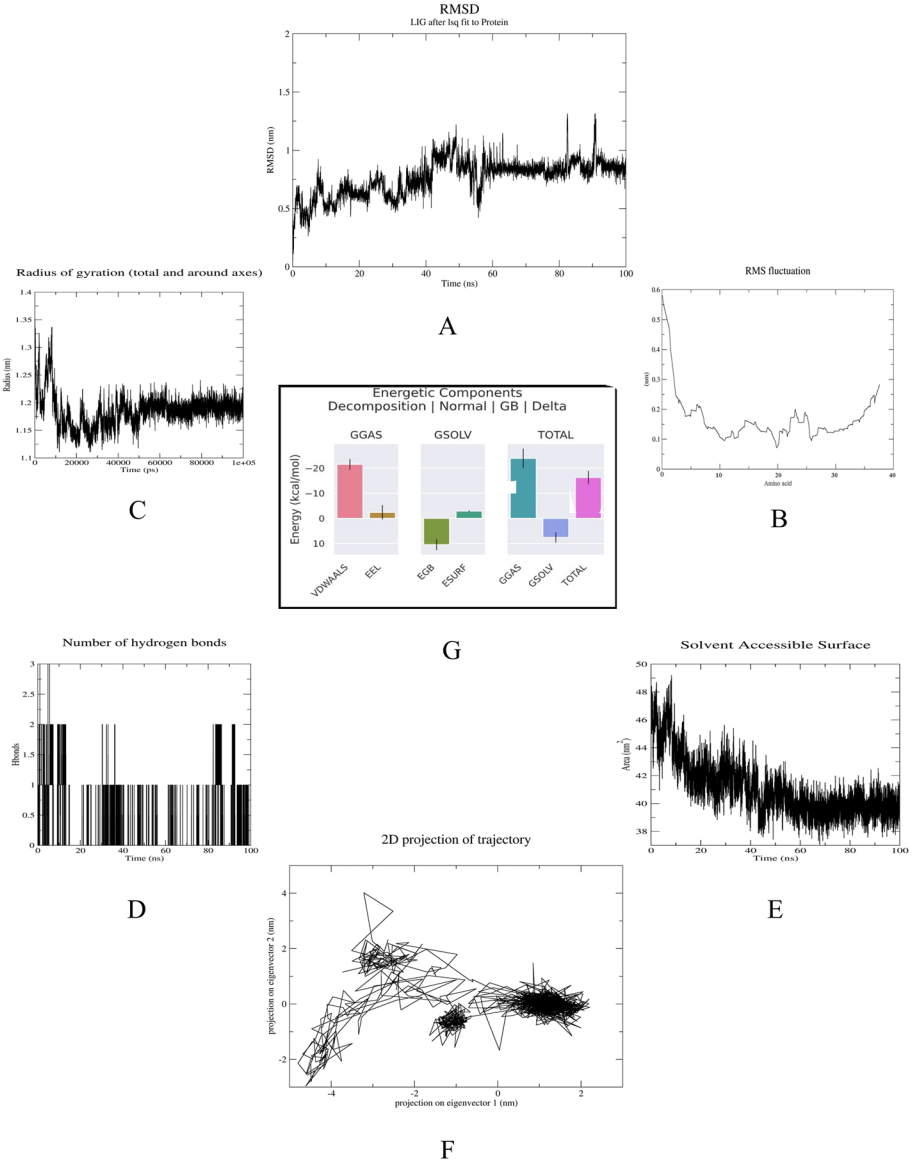

Fig. 5 Molecular dynamics simulation analysis of the Proteinaceous allergens (A6) with Paeoniflorigenone complex over 100 ns at 300 K showing (**A**) RMSD of the Cα backbone, (**B**) RMSF of residues, (**C**) radius of gyration (Rg), (**D**) hydrogen bond analysis, (**E**) solvent accessible surface area (SASA), (**F**) principal component analysis (PCA) with 2D trajectory projection, and (**G**) MM/GBSA binding energy analysis

3.7 The molecular mechanics/generalized born surface area (MM/GBSA) investigation of Paeoniflorigenone with A6, A10 and Albiflorin with 2TLR, 4TLR

The Molecular Mechanics/Generalized Born Surface Area (MM/GBSA) analysis (Fig. 5) displayed with a ΔG_bind of roughly − 16 kcal/mol, that the binding of paeoniflorigenone with A6 is thermodynamically favorable. Strong gas-phase interactions (GGAS ≈ − 24 kcal/mol), mainly from van der Waals forces (≈ − 20 kcal/mol), that reflect effective shape complementarity and hydrophobic packing, are the fundamental drivers of stability. The electrostatic contribution (approximately + 2–3 kcal/mol) is insignificant and slightly unfavorable. Favorable non-polar solvation (ESURF ≈ − 3 kcal/mol) partially offsets an unfavorable solvation energy (GSOLV ≈ + 8 kcal/mol), that is mostly caused by polar solvation (EGB ≈ + 10 kcal/mol). Desolvation penalties are generally overcome by

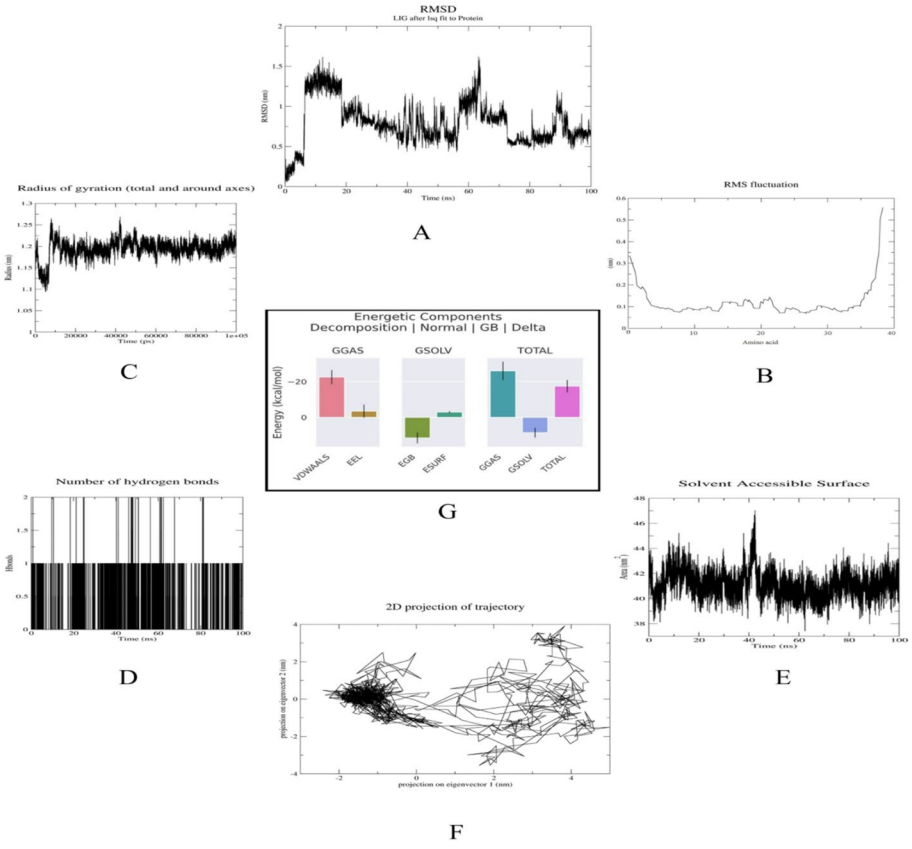

Fig. 6 Molecular dynamics simulation analysis of the Proteinaceous allergens (A10) with Paeoniflorigenone complex over 100 ns at 300 K showing (**A**) RMSD of the Cα backbone, (**B**) RMSF of residues, (**C**) radius of gyration (Rg), (**D**) hydrogen bond analysis, (**E**) solvent accessible surface area (SASA), (**F**) principal component analysis (PCA) with 2D trajectory projection, and (**G**) MM/GBSA binding energy analysis

favorable direct interactions, stabilizing the complex. The Molecular Mechanics/Generalized Born Surface Area (MM/GBSA) analysis (Fig. 6) displayed with a ΔG_bind of roughly − 17 to − 18 kcal/mol, that the binding of paeoniflorigenone with A10 is thermodynamically favorable. Strong gas-phase interactions (GGAS ≈ − 25 kcal/mol), mainly from van der Waals forces (≈ − 20 kcal/mol), that reflect effective shape complementarity and hydrophobic packing, are the fundamental drivers of stability. The electrostatic contribution (approximately + _ ≈ + 3–4 kcal/mol) is insignificant and slightly unfavorable. Favorable non-polar solvation (ESURF ≈ ≈ − 2 to − 3 kcal/mol) partially offsets an unfavorable solvation energy (GSOLV ≈ ≈ + 8–10 kcal/mol kcal/mol), that is mostly caused by polar solvation (EGB ≈ _ + 12 kcal/mol).

Desolvation penalties are generally overcome by favorable direct interactions, stabilizing the complex. The Molecular Mechanics/Generalized Born Surface Area (MM/GBSA) analysis (Fig. 7) showed that the Albiflorin with TLR2 complex exhibits strong thermodynamic stability, with an overall binding free energy (ΔG_bind) of approximately − 48 kcal/mol. This favorable binding is mainly driven by strong gas-phase interactions (GGAS ≈ − 72 kcal/mol). The dominant contribution arises from van der Waals forces (≈ − 52 kcal/mol), indicating excellent shape complementarity and substantial hydrophobic interactions within the binding pocket. Additionally, the electrostatic component (≈ − 18 kcal/mol) contributes significantly, suggesting stabilizing hydrogen bonding and Coulombic interactions. However, binding is opposed by an

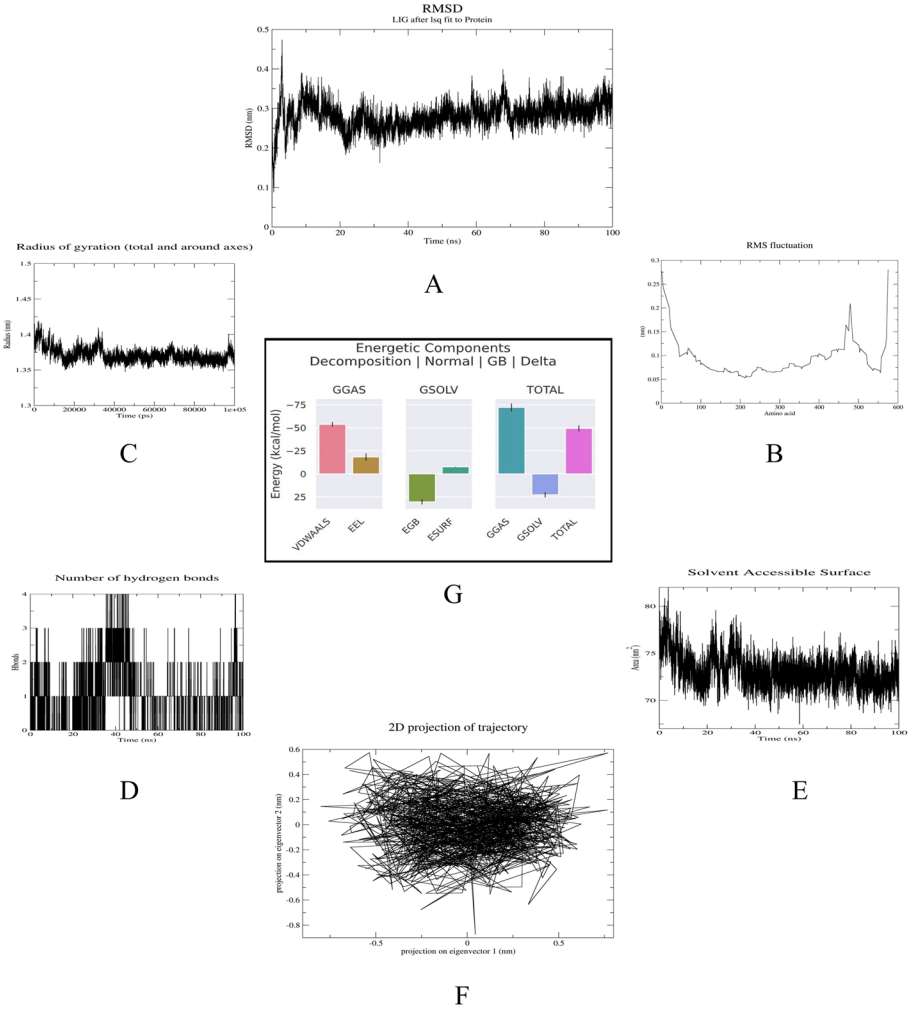

Fig. 7 Molecular dynamics simulation analysis of the TLR2 with Albiflorin complex over 100 ns at 300 K showing (**A**) RMSD of the Cα backbone, (**B**) RMSF of residues, (**C**) radius of gyration (Rg), (**D**) hydrogen bond analysis, (**E**) solvent accessible surface area (SASA), (**F**) principal component analysis (PCA) with 2D trajectory projection, and (**G**) MM/GBSA binding energy analysis

insignificant solvation energy (GSOLV ≈ + 24 kcal/mol), largely due to polar solvation (EGB ≈ + 30 kcal/mol). This desolvation penalty is partially compensated by favorable non-polar solvation (ESURF ≈ – 6 kcal/mol).

Overall, strong direct favorable molecular interactions overcome solvation costs, resulting in a stable complex. The Molecular Mechanics/Generalized Born Surface Area (MM/GBSA) analysis (Fig. 8) displayed that the Albiflorin with TLR4complex exhibits favorable thermodynamic stability, with an overall binding energy (ΔG_bind) of approximately – 30 kcal/mol. The binding affinity is mainly driven by strong gas-phase interactions (GGAS ≈ – 58 kcal/mol). Among these, van der Waals interactions (≈ – 35 kcal/mol) showed a major stabilizing contribution, indicating good shape complementarity and hydrophobic packing within the binding pocket. The electrostatic component (≈ – 22 kcal/mol) also contributes significantly and favourably, suggesting the involvement of hydrogen bonding and Coulombic interactions. However, binding is counterbalanced by an unfavorable solvation energy (GSOLV ≈ + 28 kcal/mol), primarily due to polar solvation (EGB ≈ + 35 kcal/mol). This desolvation penalty is partially offset by

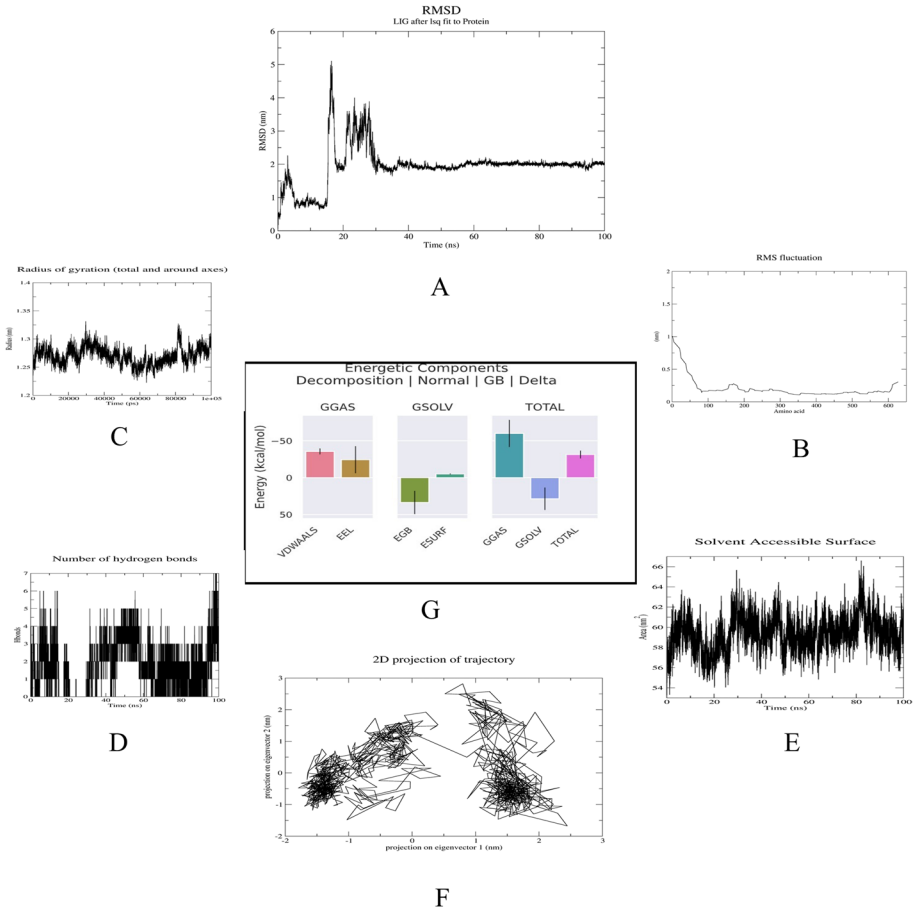

Fig. 8 Molecular dynamics simulation analysis of the TLR4 with Albiflorin complex over 100 ns at 300 K showing (**A**) RMSD of the Cα backbone, (**B**) RMSF of residues, (**C**) radius of gyration (Rg), (**D**) hydrogen bond analysis, (**E**) solvent accessible surface area (SASA), (**F**) principal component analysis (PCA) with 2D trajectory projection, and (**G**) MM/GBSA binding energy analysis

favorable non-polar solvation (ESURF ≈ – 5 kcal/mol). Overall, the strong direct intermolecular interactions surpass the solvation penalty, resulting in a stable and energetically favorable complex.

4 Discussion

Allergic disorders such as asthma, rhinitis, dermatitis, and food allergies affect over 30% of the global population and continue to the rise worldwide [1–3]. These conditions are primarily triggered by proteinaceous allergens that induce IgE-mediated hypersensitivity reactions [4, 5]. Allergens originate from diverse sources such as bacteria, fungi, plants, and animals, reflecting broad exposure risks [6, 7]. In this study, 62 allergenic protein sequences from animals were retrieved from UniProt and aligned using Clustal Omega to identify conserved motifs. Sequences corresponding to conserved pockets were taken and homology models were generated using SWISS-MODEL, and only models with more than 90% of residues in the favored regions of the Ramachandran plot were retained. Structural similarity was assessed using RMSD in PyMOL, with the lowest RMSD models chosen as experimental data sets. 13 structures from proteins such as P30922, P49822, P35747, P02769, Q7YS85, and P49064 were finalized for molecular docking. A set of 51 phytochemicals with anti-allergic or anti-inflammatory activity was

compiled and screened for ADMET properties using ADMETlab 2.0. Six compounds Albiflorin, Paeoniflorigenone, Epicatechin, Kaempferol, Tectorigenin, and Hydrobromide showed favorable profiles and were docked against the allergen models. Docking results revealed 78 interactions, with Albiflorin and Paeoniflorigenone consistently showing the most favorable binding affinities (ΔG up to − 7.1 ± 0.2 kcal/mol). Subsequently, 26 molecular dynamics (MD) simulations were performed for Albiflorin and Paeoniflorigenone complexes using GROMACS 2021. RMSD and RMSF analyses over 100 ns demonstrated that these phytochemicals formed stable complexes with the allergen proteins, maintaining key hydrogen bonds and hydrophobic interactions. Minimal RMSF deviations indicated conserved structural integrity. These findings support Albiflorin and Paeoniflorigenone as promising leads for anti-allergic drug development. A comprehensive in silico investigation was conducted to evaluate the anti-allergic potential of 51 phytochemicals based on ADMET screening, molecular docking, and molecular dynamics (MD) simulations. Among them, six compounds, including Albiflorin, Paeoniflorigenone, Epicatechin, Kaempferol, Tectorigenin, and Hydrobromide, demonstrated favorable ADMET properties. Docking analyses revealed 78 ligand–protein interactions, with Albiflorin and Paeoniflorigenone exhibiting the most favorable binding affinities (ΔG up to − 7.1 kcal/mol). MD simulations using GROMACS 2021 over a 100 ns period confirmed the stability of these interactions. Root-mean-square deviation (RMSD) and root-mean-square fluctuation (RMSF) analyses showed that the complexes remained structurally stable with minimal fluctuations, preserving critical hydrogen bonding and hydrophobic interactions. These computational findings are supported by recent experimental studies [61] demonstrated Albiflorin's ability to attenuate inflammation via modulation of the NF-κB/NLRP3 pathway in methotrexate-induced enteritis. Similarly, Albiflorin was found to reduce oxidative stress and inflammation in osteoarthritic models, further validating its pharmacological efficacy [62]. Kaempferol, another lead compound, is well-documented for its anti-allergic effects, including inhibition of mast cell activation, cytokine release, and modulation of Th1/Th2 immune responses [63, 64]. These findings align with [65], who reviewed the anti-inflammatory properties of polyphenols like Kaempferol in respiratory allergies. Several studies already reported that Albiflorin and Paeoniflorin a bioactive compound mostly from *Paeonia lactiflora*, exhibits antitumor, anti-inflammatory, and antiallergic effects. According to our ADMET studies, Paeoniflorin should be handled safely because it showed slightly Skin sensitization and eye irritation (EI). It alleviates dermatitis and urticaria by inhibiting IL-23, IFN-γ, and NF-κB/IκBα signalling, while enhancing autophagy through the LKB1/AMPK-α pathway [38, 66–69]. Docking results showed that active compound ligands modulate inflammatory cascades through TLR2 and TLR4. Molecular dynamic simulation and MM\GBSA analysis both concluded the stability and showed favorable binding affinity of Paeoniflorigenone with A6 (sp|P02769|ALBU_BOVIN: *Bos taurus*) and A10 (sp|P49822|ALBU_CANLF *Canis familiaris*). Whereas Albiflorin resulted compact stability of the complexes with TLR2 and TLR4 specifically. Simulation analysis revealed minimal structural deviation, stable hydrogen bonding and limited motion of complex indicating structurally stable complex. Similarly, binding free energy demonstrated favorable intermolecular forces ensuring thermodynamically stable complex. These receptors critically regulate Th1/Th2 balance, vital for host survival. This study highlights key findings on signalling pathways and immunopathological features of

TLR2/TLR4-mediated responses underlying major allergic expression [70, 71]. Although most of the studies represented theoretically that Albiflorin and Paeoniflorin are highly specific to antitumor, anti-inflammatory, and antiallergic activity, but other regulating metabolic pathways and pharmacodynamic index are not studied. Collectively, these results suggested that Albiflorin and Paeoniflorigenone, supported by favorable in silico and experimental data, represent promising candidates for further development as anti-allergic therapeutics. Although our said compounds i.e. Albiflorin and Paeoniflorigenone were not validated in vitro *and* in vivo analysis but several studies showed that Albiflorin and Paeoniflorigenone both have similar anti-inflammatory effects [72]. In future, common epitopic pockets from selected animal proteinaceous allergens were previously identified and can be screened for peptide-based vaccine development. Prior to selection, these peptides should be evaluated by different parameters, including physicochemical property and antigenicity analysis, T-cell (MHC-I, MHC-II) and B-cell epitope prediction, allergenicity, toxicity, immunogenicity, BLASTp with human proteome, proteolytic cleavage, ADMET profiling, molecular docking with human antibodies, TLRs, and MHC molecules, followed by binding energy calculation and molecular dynamics simulation [73].

5 Conclusion

Allergic disorders such as asthma, rhinitis, dermatitis, and food allergies affect over 30% of the global population and are rising worldwide. These conditions are primarily triggered by proteinaceous allergens that induce IgE-mediated hypersensitivity. In this study, 62 allergenic protein sequences from animals were retrieved from UniProt, aligned with Clustal Omega to identify conserve sequence, and modelled using SWISS-MODEL. Thirteen structures were finalized for molecular docking against 51 phytochemicals which were screened through the ADMET index. Six compounds, notably Albiflorin and Paeoniflorigenone, showed favorable ADMET properties and docking affinities ($\Delta G - 6.5 \pm 0.6$ kcal/mol). Molecular dynamics simulations using GROMACS confirmed stable complexes with minimal RMSD/RMSF deviations and maintained hydrogen bonding and hydrophobic interactions. Finally, Albiflorin and Paeoniflorigenone showed favorable ADMET, docking affinity, and stable interactions confirmed by PCA and MM/GBSA analyses. Albiflorin and Paeoniflorigenone are both found in the dried root of *Paeonia lactiflora*, which is popularly used in traditional Chinese herbal therapy. These findings highlight Albiflorin and Paeoniflorigenone as promising leads for anti-allergic drug development against proteinaceous allergens from animals.

Supplementary Information

The online version contains supplementary material available at https://doi.org/10.1007/s44371-026-00649-x.

Supplementary Material 1

Supplementary Material 2

Supplementary Material 3

Acknowledgements

We are grateful to the Swami Vivekananda University, Barrackpore and Oriental Institute of Science & Technology, Purba Bardhhaman campus for providing the computational facility.

Author contributions

The Study and Method development by A.S.P; material preparation, analyzing data by N.T and D.S experiments performed N.T, D.S and S.A, interpreted the results S.S.; A.S and A.S.P; Final manuscript is written by A.S.P.

Funding
No funding to declare.

Data availability
All data analysed during this study are included in this article which is publicly available in supplementary materials of this article.

Declarations

Ethics approval
Not applicable. This article contains information and analysis of in-silico data only. This article does not involve studies with animal or human subjects performed by any of the authors. Therefore, ethical approval from an institutional ethics committee was not required.

Consent to participate
Informed consent was obtained from all individual participants included in the study.

Consent for publication
All authors consent to the publication of this manuscript.

Competing interests
The authors declare no competing interests.

Received: 19 December 2025 / Accepted: 7 April 2026
Published online: 16 April 2026

References

1. Pawankar R. Allergic diseases and asthma: a global public health concern and a call to action. World Allergy Organ J. 2014;7(1):12. https://doi.org/10.1186/1939-4551-7.
2. Asher MI, Montefort S, Björkstén B, Lai CKW, Strachan DP, Weiland SK, et al. Worldwide time trends in the prevalence of symptoms of asthma, allergic rhinoconjunctivitis, and eczema in childhood. Lancet. 2006;368(9537):733–43. https://doi.org/10.1016/S0140-6736(06)69283-0.
3. Akdis CA, Blaser K. Mechanisms of interleukin-10-mediated immune suppression. Allergy. 2000;55(6):522–30. https://doi.org/10.1034/j.1398-9995.2000.00120.x.
4. Pomés A. Relevant B cell epitopes in allergic disease. Int Arch Allergy Immunol. 2010;152(1):1–11. https://doi.org/10.1159/000260078.
5. Aalberse RC. Structural biology of allergens. J Allergy Clin Immunol. 2000;106(2):228–38. https://doi.org/10.1067/mai.2000.108434.
6. Mari A. When does a protein become an allergen? Searching for a dynamic definition based on most advanced technology tools. Clin Exp Allergy. 2008;38(7):1089–94. https://doi.org/10.1111/j.1365-2222.2008.03011.x.
7. Chapman MD, Pomés A, Breiteneder H, Ferreira F. Nomenclature and structural biology of allergens. J Allergy Clin Immunol. 2007;119(2):414–20. https://doi.org/10.1016/j.jaci.2006.11.001.
8. Bush RK, Stave GM. Laboratory animal allergy: an update. ILAR J. 2003;44(1):28–51.
9. Pecquet C. New pets and allergies. Eur J Dermatol. 2012;22(1):14–22.
10. Díaz-Perales A, González-de-Olano D, Pérez-Gordo M, Pastor-Vargas C. Allergy to uncommon pets: new allergies but the same allergens. Front Immunol. 2013;4:492.
11. Wallace DV, Dykewicz MS, Bernstein DI, et al. The diagnosis and management of rhinitis: an updated practice parameter. J Allergy Clin Immunol. 2008;122(2 Suppl):S1–84. https://doi.org/10.1016/j.jaci.2008.06.003.
12. Canonica GW, Cox L, Pawankar R, Baena-Cagnani CE, Blaiss M, Bonini S, et al. Sublingual immunotherapy: World Allergy Organization position paper 2013 update. World Allergy Organ J. 2014;7(1):6. https://doi.org/10.1186/1939-4551-7-6.
13. Akdis M, Akdis CA. Therapeutic manipulation of immune tolerance in allergic disease. Nat Rev Drug Discov. 2009;8(8):645–60. https://doi.org/10.1038/nrd2653.
14. Calderón MA, Casale TB, Togias A, Bousquet J, Durham SR, Demoly P. Allergen-specific immunotherapy for respiratory allergies: from meta-analysis to registration and beyond. J Allergy Clin Immunol. 2011;127(1):30–8. https://doi.org/10.1016/j.jaci.2010.08.024.
15. Velasco G, Campo M, Manrique OJ, Bellou A, He H, Arestides RS, et al. Toll-like receptor 4 or 2 agonists decrease allergic inflammation. Am J Respir Cell Mol Biol. 2005;32(3):218–24.
16. Taylor RC, Richmond P, Upham JW. Toll-like receptor 2 ligands inhibit Th2 responses to mite allergen. J Allergy Clin Immunol. 2006;117(5):1148–54.
17. Zhou C, Kang XD, Chen Z. A synthetic Toll-like receptor 2 ligand decreases allergic immune responses in a mouse rhinitis model sensitized to mite allergen. J Zhejiang Univ Sci B. 2008;9(4):279–85. https://doi.org/10.1631/jzus.B0730029.
18. Xu H, Shu H, Zhu J, Song J. Inhibition of TLR4 inhibits allergic responses in murine allergic rhinitis by regulating the NF-κB pathway. Exp Ther Med. 2019;18(1):761–8. https://doi.org/10.3892/etm.2019.7631.
19. Lollier V, Denery-Papini S, Brossard C, Tessier D. Meta-analysis of IgE-binding allergen epitopes. Clin Immunol. 2014;153(1):31–9. https://doi.org/10.1016/j.clim.2014.03.010.
20. Bohle B, Vieths S. Improving diagnostic and therapeutic approaches for the treatment of food allergies. J Allergy Clin Immunol. 2008;121(2):336–44. https://doi.org/10.1016/j.jaci.2007.11.023.
21. Bajorath J. Integration of virtual and high-throughput screening. Nat Rev Drug Discov. 2002;1(11):882–94. https://doi.org/10.1038/nrd941.
22. Sliwoski G, Kothiwale S, Meiler J, Lowe EW Jr. Computational methods in drug discovery. Pharmacol Rev. 2013;66(1):334–95. https://doi.org/10.1124/pr.112.007336.

23. Lionta E, Spyrou G, Vassilatis DK, Cournia Z. Structure-based virtual screening for drug discovery: principles, applications and recent advances. Curr Top Med Chem. 2014;14(16):1923–38. https://doi.org/10.2174/1568026614666140929124445.
24. Sievers F, Higgins DG. Clustal omega, accurate alignment of very large numbers of sequences. In: Russell DJ (ed) Methods Mol Biol. 2014;1079:105–116. https://doi.org/10.1007/978-1-62703-646-7_6.
25. Waterhouse A, Bertoni M, Bienert S, et al. SWISS-MODEL: homology modelling of protein structures and complexes. Nucl Acids Res. 2018;46(W1):W296–303. https://doi.org/10.1093/nar/gky427.
26. Guex N, Peitsch MC, Schwede T. Automated comparative protein structure modeling with SWISS-MODEL and Swiss-PdbViewer: a historical perspective. Electrophoresis. 2009;30(Suppl 1):S162–73. https://doi.org/10.1002/elps.200900140.
27. Hodsdon ME, Ponder JW, Cistola DP. The NMR solution structure of intestinal fatty acid-binding protein complexed with palmitate: application of a novel distance geometry algorithm. J Mol Biol. 1996;264(3):585–602. https://doi.org/10.1006/jmbi.1996.0663.
28. Zemla A. LGA: a method for finding 3D similarities in protein structures. Nucl Acids Res. 2003;31(13):3370–4. https://doi.org/10.1093/nar/gkg571.
29. Morris GM, Huey R, Lindstrom W, Sanner MF, Belew RK, Goodsell DS, et al. AutoDock4 and AutoDockTools4: automated docking with selective receptor flexibility. J Comput Chem. 2009;30(16):2785–91. https://doi.org/10.1002/jcc.21256.
30. Meng XY, Zhang HX, Mezei M, Cui M. Molecular docking: a powerful approach for structure-based drug discovery. Curr Comput Aided Drug Des. 2011;7(2):146–57. https://doi.org/10.2174/157340911795677602.
31. Kumar S, Pandey AK. Chemistry and biological activities of flavonoids: an overview. Sci World J. 2013;2013:162750. https://doi.org/10.1155/2013/162750.
32. Yao LH, Jiang YM, Shi J, Tomás-Barberán FA, Datta N, Singanusong R, et al. Flavonoids in food and their health benefits. Plant Foods Hum Nutr. 2004;59(3):113–22. https://doi.org/10.1007/s11130-004-0049-7.
33. Li Y, Yao J, Han C, Yang J, Chaudhry MT, Wang S, et al. Quercetin, inflammation and immunity. Nutrients. 2016;8(3):167. https://doi.org/10.3390/nu8030167.
34. Manach C, Scalbert A, Morand C, Rémésy C, Jiménez L. Polyphenols: food sources and bioavailability. Am J Clin Nutr. 2004;79(5):727–47. https://doi.org/10.1093/ajcn/79.5.727.
35. Williamson G. The role of polyphenols in modern nutrition. Nutr Bull. 2017;42(3):226–35. https://doi.org/10.1111/nbu.12278.
36. Zhang YJ, Gan RY, Li S, Zhou Y, Li AN, Xu DP, et al. Antioxidant phytochemicals for the prevention and treatment of chronic diseases. Molecules. 2015;20(12):21138–56. https://doi.org/10.3390/molecules201219753.
37. Cai Z, Liu J, Bian H, Cai J. Albiflorin alleviates ovalbumin-induced pulmonary inflammation in asthmatic mice. Am J Transl Res. 2019;11(12):7300–9.
38. Wang G, Cheng N. Paeoniflorin inhibits mast cell-mediated allergic inflammation in allergic rhinitis. J Cell Biochem. 2018;119(10):8636–42. https://doi.org/10.1002/jcb.27135.
39. Xiong G, Wu Z, Yi J, et al. ADMETlab 2.0: an integrated online platform for accurate and comprehensive predictions of ADMET properties. Nucl Acids Res. 2021;49(W1):W5–14. https://doi.org/10.1093/nar/gkab255.
40. Li AP. Screening for human ADME/Tox drug properties in drug discovery. Drug Discov Today. 2001;6(7):357–66. https://doi.org/10.1016/S1359-6446(01)01712-3.
41. Sievers F, Wilm A, Dineen D, Gibson TJ, Karplus K, Li W, et al. Fast, scalable generation of high-quality protein multiple sequence alignments using Clustal Omega. Mol Syst Biol. 2011;7:539. https://doi.org/10.1038/msb.2011.75.
42. Bienert S, Waterhouse A, de Beer TAP, Tauriello G, Studer G, Bordoli L, et al. The SWISS-MODEL repository: new features and functionality. Nucl Acids Res. 2017;45(D1):D313–9. https://doi.org/10.1093/nar/gkw1132.
43. Studer G, Rempfer C, Waterhouse AM, Gumienny R, Haas J, Schwede T. QMEANDisCo: distance constraints applied on model quality estimation. Bioinformatics. 2020;36(6):1765–71. https://doi.org/10.1093/bioinformatics/btz828.
44. Bertoni M, Kiefer F, Biasini M, Bordoli L, Schwede T. Modeling protein quaternary structure of homo- and hetero-oligomers beyond binary interactions by homology. Sci Rep. 2017;7:10480. https://doi.org/10.1038/s41598-017-09654-8.
45. Laskowski RA, MacArthur MW, Moss DS, Thornton JM. PROCHECK: a program to check the stereochemical quality of protein structures. J Appl Crystallogr. 1993;26(2):283–91. https://doi.org/10.1107/S0021889892009944.
46. Laskowski RA, Rullmannn JA, MacArthur MW, Kaptein R, Thornton JM. AQUA and PROCHECK-NMR: programs for checking the quality of protein structures solved by NMR. J Biomol NMR. 1996;8(4):477–86. https://doi.org/10.1007/BF00228148.
47. Schrödinger L, DeLano W. PyMOL [computer software]. 2020. Available from: http://www.pymol.org/pymol.
48. Tian W, Chen C, Lei X, Zhao J, Liang J.CASTp 3.0: computed atlas of surface topography of proteins Nucl Acids Res. 2018; 46(W1):W363–W367. https://doi.org/10.1093/nar/gky473
49. Berendsen HJC, van der Spoel D, van Drunen R. GROMACS: a message-passing parallel molecular dynamics implementation. Comput Phys Commun. 1995;91(1–3):43–56. https://doi.org/10.1016/0010-4655(95)00042-E.
50. Das S, Halder D, Jeyaprakash RS.Computational-guided approach for identification of PI3K alpha inhibitor in the treatment of hepatocellular carcinoma by virtual screening and water map analysis . J Biomol Struct Dyn. 2024;3886–3908. https://doi.org/10.1080/07391102.2023.2300131
51. O'Boyle NM, Banck M, James CA, Morley C, Vandermeersch T, Hutchison GR. Open Babel: an open chemical toolbox. J Cheminform. 2011;3:33. https://doi.org/10.1186/1758-2946-3-33.
52. Jin MS, Kim SE, Heo JY, Lee ME, Kim HM, Paik SG, Lee H, Lee JO. Crystal Structure of the TLR1-TLR2 Heterodimer Induced by Binding of a Tri-Acylated Lipopeptide . Cell. 2007;130(6):1071–1082. https://doi.org/10.1016/j.cell.2007.09.008
53. Ohto U, Yamakawa N, Akashi-Takamura S, Miyake K, Shimizu T .Structural Analyses of Human Toll-like Receptor 4 Polymorphisms D299G and T399I . J Biol Chem. 2012; 287(48):40611–40617. https://doi.org/10.1074/jbc.M112.404608
54. Harder E, Damm W, Maple J, Wu C, Reboul M, Xiang JY, et al. OPLS3: a force field providing broad coverage of drug-like small molecules and proteins. J Chem Theory Comput. 2016;12(1):281–96. https://doi.org/10.1021/acs.jctc.5b00864.
55. Harder E, Damm W, Maple J, Wu C, Reboul M, Xiang JY, Wang L, Lupyan D, Dahlgren MK, Knight JL, Kaus JW, Cerutti DS, Krilov G, Jorgensen WL, Abel R, Friesner RA. J Chem Theory Comput. 2016;12(1):281–296.https://doi.org/10.1021/acs.jctc.5b00864.
56. Valdés-Tresanco MS, Valdés-Tresanco ME, Valiente PA, Moreno E. gmx_MMPBSA: A new tool to perform end-state free energy calculations with GROMACS. J Chem Theory Comput. 2021;17(10):6281–6291.
57. Pant S, Singh M, Ravichandiran V, Murty US, Srivastava HK. Peptide-like and small-molecule inhibitors against Covid-19. J Biomol Structu Dyn. 2020;1–10.

58. Pronk S, Páll S, Schulz R, Larsson P, Bjelkmar P, Apostolov R, Shirts MR, Smith JC, Kasson PM, van der Spoel D, Hess B, Lindahl E.GROMACS 4.5: a high-throughput and highly parallel open source molecular simulation toolkit. Bioinformatics. 2013;29(7):845–854. https://doi.org/10.1093/bioinformatics/btt055
59. Kumari R, Kumar R, Open-Source Drug Discovery Consortium, Lynn A. J Chem Inform Model. 2014;54(7):1951–1962. https://doi.org/10.1021/ci500020m.
60. Halder D, Banerjee S, Biswas S, Adhikari N, Ghosh B.Molecular modeling to simulation: insights into Gaussian QSAR, molecular docking, and DFT for identification of HDAC3 inhibitors for neurocognitive vascular dementia. Sci Rep. 2025;15:44561. https://doi.org/10.1038/s41598-025-28304-y
61. Zhang H, Wang J, Lang W, Liu H, Zhang Z, Wu T. Albiflorin ameliorates inflammation and oxidative stress by regulating the NF-κB/NLRP3 pathway in methotrexate-induced enteritis. Int Immunopharmacol. 2022;109:108824. https://doi.org/10.1016/j.intimp.2022.108824.
62. Zhang H, Liu H, Wang J, Zhao Y, Zhang Z, Wu T. Albiflorin alleviation efficacy in osteoarthritis injury using in vivo and in vitro models. J Pharm Pharmacol. 2024;75(10):1332–44.
63. Cheng Z, Zhang L, Yang Y, Wang Y. Anti-inflammatory and anti-allergic potential of dietary flavonoids: a review. Biomed Pharmacother. 2022;156:113945. https://doi.org/10.1016/j.biopha.2022.113945.
64. Fernández A, Pérez-González A, Alonso-González C. Natural products for the treatment of allergic rhinitis: focus on cellular signaling pathways and pharmacological targets. Front Pharmacol. 2024;15:113945. https://doi.org/10.3389/fphar.2024.113945.
65. Kumari M, Siddiqui MA, Gupta A. Recent advancement and novel application of natural polyphenols for the treatment of allergy asthma. Crit Rev Immunol. 2023;43(4):29–41.
66. Wu X, Qi X, Wang J, Zhang Y, Xiao Y, Tu C, et al. Paeoniflorin attenuates the allergic contact dermatitis response via inhibiting the IFN-γ production and the NF-κB/IκBα signaling pathway in T lymphocytes. Int Immunopharmacol. 2021;96:107687. https://doi.org/10.1016/j.intimp.2021.107687.
67. Guo J, Peng L, Zeng J, Zhang M, Xu F, Zhang X, et al. Paeoniflorin suppresses allergic and inflammatory responses by promoting autophagy in rats with urticaria. Exp Ther Med. 2021;21(6):590. https://doi.org/10.3892/etm.2021.10022.
68. Sun S, Jimu RB, Lema AK, Elmamoune H, Fan Z, Jin C, et al. A systematic review on the origin, anti-inflammatory effect, mechanism, pharmacokinetics, and toxicity of albiflorin. Arab J Chem. 2024;17(7):105836. https://doi.org/10.1016/j.arabjc.2024.105836.
69. Li GR, Xia GY, Zhou LN, Xia H, Wei XH, Lin PC, et al. Albiflorin: a promising natural monoterpene glycoside with potential therapeutic benefits for multiple physiological systems. Food Med Homol. 2025;2:9420064. https://doi.org/10.1093/fmh/9420064.
70. Mukherjee S, Karmakar S, Babu SP. TLR2 and TLR4 mediated host immune responses in major infectious diseases: a review. Braz J Infect Dis. 2016;20(2):193–204. https://doi.org/10.1016/j.bjid.2015.10.011.
71. Durai P, Shin HJ, Achek A, Kwon HK, Govindaraj RG, Panneerselvam S, et al. Toll-like receptor 2 antagonists identified through virtual screening and experimental validation. FEBS J. 2017;284(14):2264–83. https://doi.org/10.1111/febs.14124.
72. Wang QS, Gao T, Cui YL, Gao LN, Jiang HL. Comparative studies of paeoniflorin and albiflorin from Paeonia lactiflora on anti-inflammatory activities. Pharm Biol. 2014;52(9):1189–1195. https://doi.org/10.3109/13880209.2014.880490
73. Stalker MR, Grant J, Yong CW, Ohene-Yeboah LA, Mays TJ, Parker SC.Molecular simulation of hydrogen storage and transport in cellulose. Mol Simul. 2021;47(2–3). https://doi.org/10.1080/08927022.2019.1593975

Publisher's Note